Received: 8 October 2022 | Accepted: 6 December 2022

DOI: 10.1002/pamm.202200252

A 3rd/2nd order MOOD limited scheme for the shallow water equations

Sophie Hörnschemeyer[1,*], **Paola Bacigaluppi**[2,**], **Sebastian Noelle**[1,***], and **Guoxian Chen**[3,4,†]

[1] Institute for Geometry and Practical Mathematics, RWTH Aachen University, Aachen, Germany
[2] Department of Aerospace Science and Technology, Politecnico di Milano, Milan, Italy
[3] School of Mathematics and Statistics, Wuhan University, Wuhan, 430072, P.R. China
[4] Computational Science Hubei Key Laboratory, Wuhan University, Wuhan, 430072, P.R. China

We present a high-order accurate, positivity-preserving and well-balanced finite volume scheme for the shallow water equations with variable topography. An unlimited third-order scheme is combined with the recent, second-order accurate Bottom-Surface-Gradient Method (BSGM, [5]). This is monitored by an a-posteriori MOOD (Multidimensional Optimal Order Detection) limiting step [2, 7–9], which detects possible local instabilities of a high-order candidate solution such as loss of positivity or local oscillations, and switches locally to a lower order, stable and robust "parachute" scheme if necessary. We demonstrate the accuracy, effectiveness and robustness of the proposed adaptive methodology with numerical experiments, both for near-equilibrium and non-equilibrium depth-averaged flows.

1 Introduction

We consider the one-dimensional shallow water equations

$$\partial_t U + \partial_x F(U) = S(U, x) \tag{1.1}$$

with

$$U = \begin{pmatrix} h \\ hu \\ hv \end{pmatrix}, \quad F(U) = \begin{pmatrix} hu \\ hu^2 + \frac{g}{2}h^2 \\ huv \end{pmatrix}, \quad \text{and} \quad S(U) = \begin{pmatrix} 0 \\ -gh\partial_x b \\ 0 \end{pmatrix}, \tag{1.2}$$

where h is the water height, (u, v) is the velocity field, the bottom topography is given by b and the gravitational acceleration by g. The shallow water equations are the standard model for free surface flows and are used to model the flow in rivers, lakes and oceans. This work is part of a larger project in which we plan to couple upwelling in multi-layer ocean currents with phytoplankton dynamics (NPZD), see e.g. [6]. Therefore our aim is to develop a simple, flexible, robust and high-order flow solver which can be extended to multiphysics.

Our numerical approximation combines a standard third-order accurate and the recent, well-balanced and positivity preserving second-order accurate finite volume scheme [5]. The switch is monitored by a number of ad-hoc indicators which have been used successfully in the MOOD community since the original work [8, 9] for conservation laws, and extended recently to the shallow water equations in [10, 12]. Note that there are other well established and sophisticated detectors of regularity based, for example, on multi-resolution analysis [11, 13] or on a-posteriori error estimates [15]. There is also a multitude of recent schemes proposing sophisticated well-balanced schemes, see e.g. [1, 4, 5, 10, 12, 14] and the references therein.

The aim of this contribution is to clarify if a second-order accurate scheme can be robust enough to serve as a parachute. Our approach is closely related to [10, 12], who use a first-order scheme as parachute. Instead, we choose the BSGM, which is positivity-preserving, well-balanced and avoids non-physical reflections from bottom reconstructions, and is more accurate than a first-order scheme. If this stabilization should not be sufficient, we will use a first-order reserve-parachute such as [4]. Note that more generally, a "cascade" of parachutes was introduced in [2].

2 Spatial reconstruction

Let $\Omega \subset \mathbb{R}$ be a one-dimensional domain. We discretize $\Omega = \bigcup_{i\in I} C_i$ with uniform cells $C_i = (x_{i-\frac{1}{2}}, x_{i+\frac{1}{2}})$ and index set $I \subset \mathbb{Z}$. For simplicity we choose a uniform discretization with $x_{i+\frac{1}{2}} - x_{i-\frac{1}{2}} = \Delta x$. We define the surface level by $w := h + b$. Let $q_i(t)$ for $q \in \{h, hu, hv, b, w\}$ be the computed cell averages.

* Corresponding author: e-mail hoernschemeyer@igpm.rwth-aachen.de, phone +49 241 80 96337
** paola.bacigaluppi@polimi.it
*** noelle@igpm.rwth-aachen.de
† gxchen.math@whu.edu.cn

2.1 Piecewise quadratic reconstruction

The third-order finite volume scheme (FV3) is based on piecewise quadratic reconstructions $\hat{q}_i(x)$ of the quantities $q \in \{b, h, hu, hv\}$ which preserve the cell averages in cell C_i and its neighbors,

$$\frac{1}{\Delta x}\int_{C_j} \hat{q}_i(x)\,dx = q_j \quad \text{for} \quad j \in \{i-1, i, i+1\}. \tag{2.1}$$

The one-sided limits of the reconstructions are given by

$$q_{i-\frac{1}{2}+} := \hat{q}_i(x_{i-\frac{1}{2}}), \quad q_{i+\frac{1}{2}-} := \hat{q}_i(x_{i+\frac{1}{2}}). \tag{2.2}$$

2.2 Piecewise linear reconstruction

To construct a second-order finite volume scheme (FV2), for each quantity $q \in \{b, w := b+h, hu, hv\}$ we define a preliminary piecewise linear reconstruction

$$\tilde{q}_i(x) := q_i + \partial_x \tilde{q}_i (x - x_i) \quad \text{for} \quad x \in C_i, \tag{2.3}$$

where $\partial_x \tilde{q}_i$ approximates the slope of q using a minmod-type limiter and x_i is the center in cell C_i. This gives preliminary one-sided limits

$$\tilde{q}_{i-\frac{1}{2}+} := \tilde{q}_i(x_{i-\frac{1}{2}}), \quad \tilde{q}_{i+\frac{1}{2}-} := \tilde{q}_i(x_{i+\frac{1}{2}}). \tag{2.4}$$

The preliminary linear reconstruction can lead to negative water heights near wet-dry fronts. A modified reconstruction of the slopes of bottom and water surface which cures the problem was recently proposed in [5]: if, for example, there is a negative water height at the left interface ($x_{i-\frac{1}{2}}$), then we correct the slopes of $q \in \{w, b\}$ by

$$\partial_x q_i := \frac{q_i - z_{i-\frac{1}{2}+}}{\Delta x/2}, \quad \text{with} \quad z_{i-\frac{1}{2}+} := w_i + \operatorname{minmod}\left(w_{i-\frac{1}{2}+} - w_i, b_{i-\frac{1}{2}+} - w_i\right). \tag{2.5}$$

This modification shifts the front from the interior to the cell interface. See [5] for the details. Table 1 summarizes the stability properties of the piecewise quadratic, linear and constant reconstructions. Only the piecewise constant and the piecewise linear BSGM reconstructions are stable enough to serve as possible parachutes.

Table 1: Stability properties of spatial reconstructions. The BSGM scheme is denoted by FV2*.

scheme	spatial reconstruction	positivity preserving	oscillation free
FV3	quadratic	no	no
FV2	minmod	no	yes
FV2*	BSGM*	yes	yes
FV1	constant	yes	yes

2.3 Hydrostatic reconstruction, numerical fluxes and source terms

The techniques reviewed in this section are independent of the type of piecewise polynomial reconstruction. To deal with the non-conservative product in the source term, we use the hydrostatic reconstruction introduced by Audusse in [1] and modified by Chen and Noelle in [4]. We calculate the hydrostatic reconstruction values for the third- and second-order scheme by

$$b^*_{i+\frac{1}{2}} := \min\left(w_{i+\frac{1}{2}-}, w_{i+\frac{1}{2}+}, \max\left(b_{i+\frac{1}{2}-}, b_{i+\frac{1}{2}+}\right)\right), \quad h^*_{i+\frac{1}{2}\pm} := \min\left(w_{i+\frac{1}{2}\pm} - b^*_{i+\frac{1}{2}}, h_{i+\frac{1}{2}\pm}\right). \tag{2.6}$$

The numerical fluxes at the cell interface are computed using the HLL-flux and the values of the hydrostatic reconstruction:

$$F_{i\pm\frac{1}{2}} := \mathcal{F}_{\text{HLL}}\left(U^*_{i\pm\frac{1}{2}-}, U^*_{i\pm\frac{1}{2}+}\right). \tag{2.7}$$

Due to the hydrostatic reconstruction we also obtain two singular source terms in addition to the inner source term. As in [4], the singular source terms for the third-order scheme and for the second-order scheme are computed by

$$S_{i-\frac{1}{2}+} := -\frac{g}{2\Delta x}\left(h^*_{i-\frac{1}{2}+} + h_{i-\frac{1}{2}+}\right)\left(b_{i-\frac{1}{2}+} - b^*_{i-\frac{1}{2}+}\right), \quad S_{i+\frac{1}{2}-} := -\frac{g}{2\Delta x}\left(h_{i+\frac{1}{2}-} + h^*_{i+\frac{1}{2}-}\right)\left(b^*_{i+\frac{1}{2}-} - b_{i+\frac{1}{2}-}\right). \tag{2.8}$$

To calculate the interior source term for the third-order scheme we use the high-order quadrature rule given in [14]:

$$S^{\text{int}}_i := \frac{4g}{6\Delta x}\cdot\left((h_{i-\frac{1}{2}+} + h_i)(b_{i-\frac{1}{2}+} - b_i) + (h_i + h_{i+\frac{1}{2}-})(b_i - b_{i+\frac{1}{2}-})\right) - \frac{g}{6\Delta x}(h_{i-\frac{1}{2}+} + h_{i+\frac{1}{2}-})(b_{i-\frac{1}{2}+} - b_{i+\frac{1}{2}-}). \tag{2.9}$$

For the second-order scheme, we calculate the interior source term as in [4, 5] by

$$S^{\text{int}}_i := -\frac{g}{2\Delta x}(h_{i-\frac{1}{2}+} + h_{i+\frac{1}{2}-})(b_{i+\frac{1}{2}-} - b_{i-\frac{1}{2}+}). \tag{2.10}$$

3 Finite Volume Update

The semidiscrete scheme for the approximated cell averages $U_i(t)$ is given by

$$\frac{d}{dt}U_i(t) = \mathcal{H}_i, \tag{3.1}$$

where the spatially high-order accurate discrete operator $\mathcal{H}$ is given by

$$\mathcal{H}_i := -\frac{1}{\Delta x}\big(F_{i+\frac{1}{2}} - F_{i-\frac{1}{2}}\big) + S_{i-\frac{1}{2}+} + S_i^{\text{int}} + S_{i+\frac{1}{2}-}. \tag{3.2}$$

The first-order in time, higher-order in space fully discrete scheme reads

$$U^{n+1} = U^n + \Delta t\mathcal{H}(U^n), \tag{3.3}$$

where U^n represents the vector $(U_i^n)_{i\in I}$. We discretize (3.3) in time with the third-order accurate strong stability preserving Runge-Kutta scheme of Shu and Osher, where the Runge-Kutta stages $U^{n,(s)}$ and the update are given by

$$U^{n+1} := \frac{U^n + 2U^{n,(3)}}{3} \quad \text{with} \quad \begin{cases} U^{n,(0)} & := U^n, \\ U^{n,(1)} & := U^n + \Delta t\mathcal{H}(U^n), \\ U^{n,(2)} & := U^{n,(1)} + \Delta t\mathcal{H}(U^{n,(1)}), \\ U^{n,(3)} & := U^{n,(2)} + \Delta t\mathcal{H}\Big(\frac{3U^n+U^{n,(2)}}{4}\Big). \end{cases} \tag{3.4}$$

Depending on the choice of spatial reconstruction, (3.2) - (3.3) define the FV3 respectively the BSGM scheme. It is well-known that under the standard CFL-condition

$$\frac{\Delta t}{\Delta x}\max\left(|u^n_{i+\frac{1}{2}\pm}| + \sqrt{gh^n_{i+\frac{1}{2}\pm}}\right) \le \frac{1}{2} \tag{3.5}$$

the FV3 scheme is third-order accurate for smooth solutions. It also preserves still water, but it is neither well-balanced nor positivity-preserving near wet-dry fronts, and may create overshoots at discontinuities. Clearly, the FV3 scheme needs additional stabilization, which we explore in the MOOD framework. The recent contributions [10, 12] use the first-order FV1 scheme as parachutes, since a traditional FV2 scheme has its own stability issues. On the other hand, it was proven in [5] that the new second-order BSGM also satisfies a number of crucial stability properties:

Theorem 3.1 *Under the CFL-condition* (3.5) *the BSGM is second-order accurate, well-balanced and positivity-preserving and avoids non-physical reflections from bottom reconstructions.*

These properties, as well as the built-in minmod stabilization, make the BSGM scheme an interesting, more slim, and perhaps less disruptive candidate for our parachute.

4 MOOD

The previous sections proposed a high-order scheme that is also well-balanced. However, this unlimited high-order scheme is not able to preserve the non-negativity of the water height and may create oscillations in the vicinity of shocks. The presented second-order BSGM instead is positivity-preserving, well-balanced and does not create oscillations. Our aim is now to combine these two schemes to get a high-order accurate and robust scheme. For this purpose we use the MOOD approach [7–9] which is an a-posteriori limiting process and works as follows:

Suppose that the high-order, unlimited candidate solution $U^{(s)}_{\text{FV3}}$ at stage $s = 1, 2, 3$ of the Runge-Kutta scheme has already been computed. We check the physical and numerical admissibility of the candidate solution locally, by using the detectors described below. If the candidate solution does verify all the checks, we will set $U^{n,(s)} := U^{(s)}_{\text{FV3}}$. Otherwise, if one of the admissibility criteria is not fulfilled, a cell is flagged and the solution is locally recomputed using the second-order BSGM scheme, which hereafter will be referred to as parachute, and we set $U^{n,(s)} := U^{(s)}_{\text{BSGM}}$ and proceed with the next stage (3.4).

4.1 Detectors

We use the following detection criteria that were inspired by the works [2, 3, 8, 9]. Figure 1 displays the detector chain.

Physical admissibility detector (PAD) The PAD determines whether the solution is physically admissible. In the case of the shallow water equations this criterium fails within the cell C_i if the water height is negative:

$$\text{PAD}_i = \begin{cases} 1, & \text{if} \quad h^{(s)}_{\text{FV3},i} < 0, \\ 0, & \text{else.} \end{cases} \tag{4.1}$$

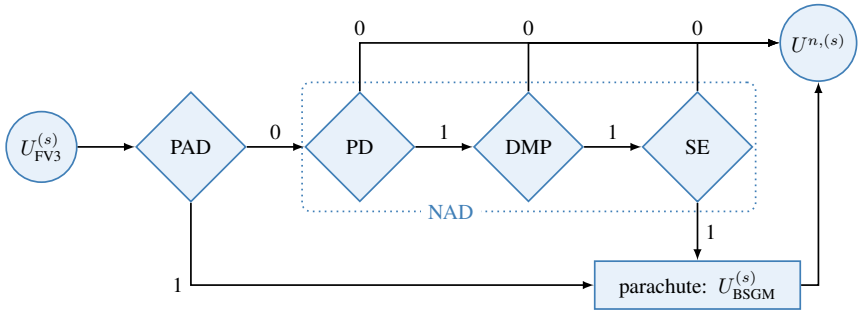

Fig. 1: Schematic illustration of the detection process. Note that 1 always means the detector is activated.

Numerical admissibility detector (NAD) The NAD checks for each component $q \in \{h, hu, hv\}$ of the candidate solution $U^{(s)}_{\text{FV3},i}$ if there arise numerical oscillations that have to be corrected. Let $N(i) := \{i-1, i, i+1\}$ be the neighborhood of cell C_i. For $s = 1, 2, 3$ define

$$m_i(q) := \min_{j \in N(i)} (q_j^{n,(s-1)}), \quad M_i(q) := \max_{j \in N(i)} (q_j^{n,(s-1)}). \tag{4.2}$$

The NAD now consists of three steps [2, 3]:

- **PD** (plateau): The first detector is activated in cell C_i if there was no plateau region in the time step before.

$$\text{PD}_i(q) = \begin{cases} 1, & \text{if} \quad M_i(q) - m_i(q) \geq \Delta x^3, \\ 0, & \text{else.} \end{cases} \tag{4.3}$$

- **DMP** (relaxed discrete maximum principle): In case the PD is activated, the next criterium determines if the candidate solution fulfilles a relaxed discrete maximum principle. We allow the solution to overshoot the old extrema a little bit.

$$\text{DMP}_i(q) = \begin{cases} 0, & \text{if} \quad m_i(q) - \varepsilon < q^{(s)}_{\text{FV3},i} < M_i(q) + \varepsilon, \\ 1, & \text{else.} \end{cases} \tag{4.4}$$

with

$$\varepsilon := 10^{-3}(M_i(q) - m_i(q)). \tag{4.5}$$

As in [2] in this criterium the value of ε is chosen in such a way that the candidate solution is allowed to overshoot the previous extrema by a small fraction of the total jump.

- **SE** (smooth extrema): If a component $q^{(s)}_{\text{FV3}}$ of the candidate solution $U^{(s)}_{\text{FV3}}$ violates the DMP within the cell C_i the next detector checks if the new extremum is smooth. As done in [8, 9] we compute a preliminary quadratic polynomial reconstruction $\hat{q}_{\text{FV3}}$ based on the values $q^{(s)}_{\text{FV3}}$. Then we define the second derivative $\mathcal{X}_i := \partial_{xx}\hat{q}_{\text{FV3},i}$ and the maximal and minimal curvatures

$$\mathcal{X}_i^{\max} := \max_{j \in N(i)} (\mathcal{X}_j) \quad \text{and} \quad \mathcal{X}_i^{\min} := \min_{j \in N(i)} (\mathcal{X}_j). \tag{4.6}$$

We call an extremum smooth if the minimal and maximal curvature have the same sign so that there are no turning points, and if the curvatures are "close" enough. Then the smoothness criterium is defined by

$$\text{SE}_i = \begin{cases} 0, & \text{if} \quad \mathcal{X}_i^{\max}\mathcal{X}_i^{\min} > 0 \quad \text{and} \quad \left|\frac{\mathcal{X}_i^{\min}}{\mathcal{X}_i^{\max}}\right| \leq \frac{1}{2}, \\ 1, & \text{else.} \end{cases} \tag{4.7}$$

If this criterium fails, the solution has to be recomputed locally using the BSGM parachute scheme.

To summarize, the NAD is given by

$$\text{NAD}_i = \text{PD}_i \, \text{DMP}_i \, \text{SE}_i \tag{4.8}$$

and we choose the solution to be

$$U_i^{n,(s)} = \begin{cases} U^{(s)}_{\text{BSGM},i}, & \text{if} \quad \text{PAD}_i = 1 \quad \text{or} \quad \text{NAD}_i = 1, \\ U^{(s)}_{\text{FV3},i}, & \text{else.} \end{cases} \tag{4.9}$$

4.2 Correction of fluxes and singular source terms in unlimited neighbor cells

After having detected a trouble cell, the finite volume update in this cell will be recomputed. Due to the piecewise linear reconstruction used in this cell now, the values at the cell interfaces change and so does the value of the hydrostatic reconstruction. This creates an issue at the interfaces between flagged and unflagged cells. To stay conservative we have to recompute the flux and the singular source term at this interface in the unflagged cell. Using the new value of the hydrostatic reconstruction in (2.7) and (2.8), respectively, yields the corrected flux and the corrected singular source term, named by $F^{\text{corr}}_{i\pm\frac{1}{2}}$ and $S^{\text{corr}}_{i\pm\frac{1}{2}\pm}$, respectively. If, for example, the solution in cell C_i has to be recomputed using the BSGM and the high-order candidate solution in cell C_{i-1} (resp. C_{i+1}) can be kept, for $s = 1, 2, 3$ we compute

$$U^{n,(s)}_{i-1} = U^{n,(s-1)}_{i-1} - \frac{\Delta t}{\Delta x}\big(F^{\text{corr}}_{i-\frac{1}{2}} - F^{\text{FV3}}_{i-\frac{3}{2}}\big) + \Delta t\big(S^{\text{FV3}}_{i-\frac{3}{2}+} + S^{\text{FV3}}_{i-1} + S^{\text{corr}}_{i-\frac{1}{2}-}\big) \quad \text{and} \tag{4.10}$$

$$U^{n,(s)}_{i+1} = U^{n,(s-1)}_{i+1} - \frac{\Delta t}{\Delta x}\big(F^{\text{FV3}}_{i+\frac{3}{2}} - F^{\text{corr}}_{i+\frac{1}{2}}\big) + \Delta t\big(S^{\text{corr}}_{i+\frac{1}{2}+} + S^{\text{FV3}}_{i+1} + S^{\text{FV3}}_{i+\frac{3}{2}-}\big) \quad \text{respectively.} \tag{4.11}$$

Theorem 4.1 *Under the CFL-condition* (3.5)*, the third/second-order MOOD scheme is positivity-preserving and well-balanced for the lake at rest.*

Proof. Suppose a lake at rest is given at time t^n. Away from flagged cells we use the unlimited FV3 scheme that is well-balanced. In a region of flagged cells we use the BSGM that is also well-balanced. Thus, to show the well-balanced property of the MOOD scheme, now it is sufficient to consider only the transition between the cells corrected with the BSGM parachute and their unlimited neighbor cells with flux and source term correction as mentioned in (4.10) and (4.11). We compute the values of the quadratic reconstruction (2.2), the linear reconstruction (2.3) with BSGM-correction (2.5), and the resulting hydrostatic reconstruction (2.6). We use these values to calculate the fluxes (2.7) and the source terms (2.8) – (2.10). It yields that the residual $\mathcal{H}_i$ in (3.2) vanishes both in the flagged cell that was computed using the BSGM and in the unlimited neighbor cell. Thus, the MOOD scheme is well-balanced. □

5 Numerical examples

If h, u and b are constant and $v = v(x,t)$ the shallow water equations reduce to the linear advection equation. For smooth initial data, the detectors do not strike in any cell. In this case, we get third-order convergence, see Figure 2. If we flag either one or five cells by hand the scheme still converges at full rate in the L^1 norm, and at order 1.7 in L^∞.

Next we study the advection of a step function. We compared the results of the MOOD scheme with the unlimited third-order scheme and the second-order BSGM. The results of the different schemes are plotted in Figure 3. The solution of the MOOD scheme is much sharper than that of the BSGM and does not produce oscillations at the shock as does the unlimited FV3. We compared this scheme also with a third-order scheme that was equipped with a first-order parachute scheme but at least in this test example, no significantly better accuracy could be detected by using the BSGM parachute.

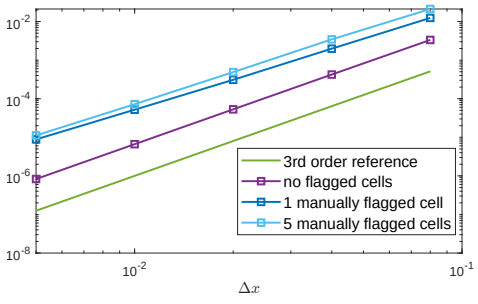

Fig. 2: L^1 convergence for smooth advection.

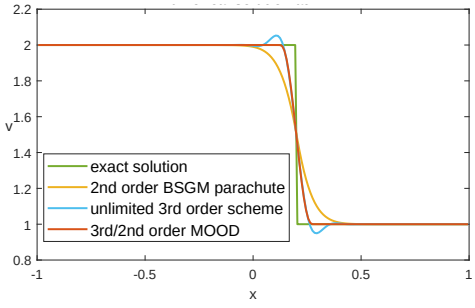

Fig. 3: Advection of a discontinuity.

In the next example, we study perturbations of a lake at rest. The computational domain is $\Omega = [0, 4]$ and is discretized with 200 cells. We use periodic boundary conditions. The bottom topography is a volcano crater given by

$$b(x) = \begin{cases} 1 - 0.8e^{-r}, & r < \ln(8/5), \\ 0.8e^{-r}, & \text{otherwise} \end{cases} \quad \text{with} \quad r := 2(x-2)^2. \tag{5.1}$$

We set the water level to 0.45 in the interior and 0.3 in the exterior of the crater. The scheme preserves the lake-at-rest equilibrium to machine accuracy. Next we add a step of size 0.03 to the water level in the interval $[-0.25, 0.25]$ (note that the boundary conditions are periodic). The numerical solution at various times and the activated detectors are plotted in Figure 4. The initial perturbation splits and travels to the left and right, with a shock upfront and a trailing rarefaction. The NAD indicator (marked with green diamonds) flags the corners of the waves, while the PAD indicator (red circles) marks the

wet-dry fronts. It is here where the MOOD limiter switches from the high-order unlimited scheme to the parachute BSGM scheme. At time $T = 0.6$, the perturbation is approaching the volcano, and is running up its shore at $T = 0.9$. At time $T = 1.2$ it has turned around and is merging into the open water as a hydraulic jump. Not visible in the figure, the water level inside the crater is perturbed by a numerical error which has traveled across the ridge of the volcano and seems to be of the size of the numerical truncation error.

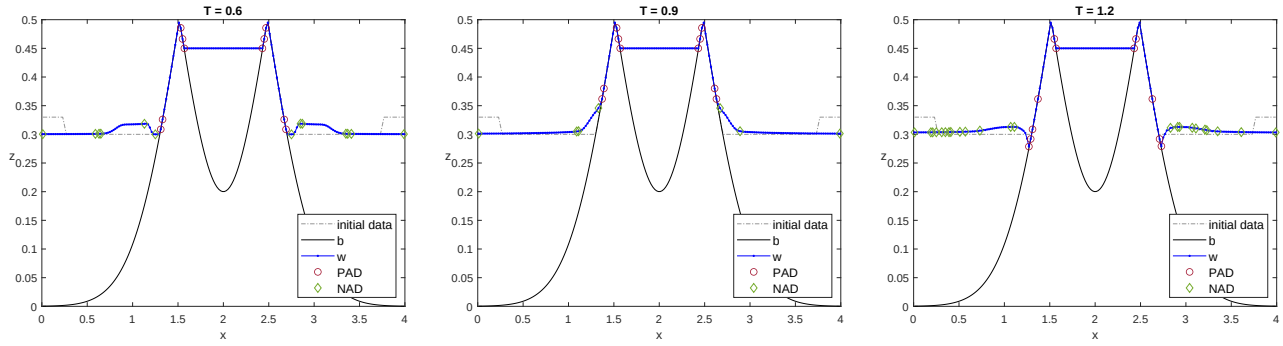

Fig. 4: Volcano test: numerical solution and activated detectors at times $T = 0.6$, $T = 0.9$ and $T = 1.2$.

6 Conclusion and outlook

We have presented preliminary results of a new MOOD-limited high-order shallow water solver. An unlimited high-order candidate solution is checked for physical and numerical admissibility using various detectors. If the candidate solution is not admissible in a cell, this cell is locally corrected with a robust parachute scheme. In contrast to previous work based on first-order parachutes [10, 12], we use the second-order accurate BSGM scheme [5] to stabilize the high-order unlimited solution. Numerical experiments provide first promising results, but the pro's and con's of different parachute schemes need to be studied in future work.

The present contribution is the first step in a larger project whose goal is to develop a simple-to-implement and robust, but high-order accurate scheme to model ocean currents coupled with phytoplankton dynamics. Work in progress includes the two-dimensional multilayer case, well-balancing moving equilibria, and coupling with an NPZD dynamical system.

Acknowledgements The work of S.H. and S.N. was supported by Deutsche Forschungsgemeinschaft under DFG grant 320021702 / GRK2326. P.B. has been supported by the MSCA EF Master Class 2019 Grant of Politecnico di Milano, and G.C. by the National Science Foundation of China (11371023). Open access funding enabled and organized by Projekt DEAL.

References

[1] E. Audusse, F. Bouchut, M.-O. Bristeau, R. Klein, and B. Perthame, SIAM J. Sci. Comput., **25(6)**, 2050–2065 (2004).
[2] P. Bacigaluppi, R. Abgrall, and S. Tokareva, submitted (2022).
[3] P. Bacigaluppi, J. Carlier, M. Pelanti, P. M. Congedo, and R. Abgrall, SIAM J. Sci. Comput., **90(1)**, 1–28 (2022).
[4] G. Chen and S. Noelle, SIAM J. Numer. Anal., **55(2)**, 758–784 (2017).
[5] G. Chen and S. Noelle, J. Comput. Phys., **467** (2022).
[6] F. Chenillat, P. Franks, P. Rivière, X. Capet, N. Grima, and B. Blanke, J. Geophys. Res. Oceans, **120(8)**, 5566–5588 (2015).
[7] S. Clain, S. Diot, and R. Loubère, J. Comput. Phys., **230(10)**, 4028–4050 (2011).
[8] S. Diot, S. Clain, and R. Loubère, Comput. & Fluids, **64**, 43–63 (2012).
[9] S. Diot, R. Loubère, and S. Clain, Internat. J. Numer. Methods Fluids, **73(4)**, 362–392 (2013).
[10] J. Figueiredo and S. Clain, J. Comput. Phys., **88(1)**, 30 (2021).
[11] N. Gerhard and S. Müller, Comput. Appl. Math., **35**, 321–349 (2016).
[12] V. Michel-Dansac, C. Berthon, S. Clain, and F. Foucher, Computers & Fluids, **230**, 21 (2021).
[13] S. Müller, Adaptive multiscale schemes for conservation laws (Springer-Verlag, 2003).
[14] S. Noelle, N. Pankratz, G. Puppo, and J. R. Natvig, J. Comput. Phys., **213(2)**, 474–499 (2006).
[15] M. Ohlberger, Internat. J. Numer. Methods Fluids, **3**, 333–354 (2009).